

Interaction of Hydrogen Chloride with Ice Surfaces: The Effects of Grain Size, Surface Roughness, and Surface Disorder

V. Faye McNeill,^{†,‡} Franz M. Geiger,^{§,||} Thomas Loerting,^{§,-} Bernhardt L. Trout,[†]
Luisa T. Molina,[§] and Mario J. Molina^{*,§,^}

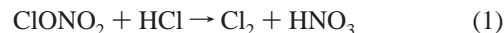
Departments of Chemistry and Earth, Atmospheric, and Planetary Sciences and Department of Chemical Engineering, Massachusetts Institute of Technology, Cambridge, Massachusetts 02139

Received: December 24, 2006; In Final Form: May 9, 2007

Characterization of the interaction of hydrogen chloride (HCl) with polar stratospheric cloud (PSC) ice particles is essential to understanding the processes responsible for ozone depletion. The interaction of HCl with ice was studied using a coated-wall flow tube with chemical ionization mass spectrometry (CIMS) between 5×10^{-8} and 10^{-4} Torr HCl and between 186 and 223 K, including conditions recently shown to induce quasi-liquid layer (QLL) formation on single crystalline ice samples. Measurements were performed on smooth and rough (vapor-deposited) polycrystalline ice films. A numerical model of the coated-wall flow reactor was used to interpret these results and results of studies on zone-refined ice cylinders with grain sizes on the order of several millimeters (reported elsewhere). We found that HCl adsorption on polycrystalline ice films typically used in laboratory studies under conditions not known to induce surface disordering consists of two modes: one relatively strong mode leading to irreversible adsorption, and one relatively weak binding mode leading to reversible adsorption. We have indirect experimental evidence that these two modes of adsorption correspond to adsorption to sites at crystal faces and those at grain boundaries, but there is not enough information to enable us to conclusively assign each adsorption mode to a type of site. Unlike what was observed in the zone-refined ice study, there was no strong qualitative contrast found between the HCl uptake curves under QLL versus non-QLL conditions for adsorption on smooth and vapor-deposited ices. We also found indirect evidence that HCl hexahydrate formation on ice between 3×10^{-7} and 2×10^{-6} Torr HCl and between 186 and 190 K is a process involving hydrate nucleation and propagation on the crystal surface, rather than one originating in grain boundaries, as has been suggested for ice formed at lower temperatures. These results underscore the dependence of the HCl–ice interaction on the characteristics of the ice substrate.

I. Introduction

It is now well-known that heterogeneous reactions of chlorine nitrate, ClONO₂, and hydrogen chloride, HCl, on the surfaces of polar stratospheric cloud (PSC) particles play a key role in stratospheric ozone depletion.^{1–3} These heterogeneous processes are referred to as “chlorine activation reactions” because their net effect is to convert the otherwise stable chlorine reservoirs ClONO₂ and HCl into chlorine gas, which in the polar spring can then be photolyzed and go on to participate in ozone destruction. HCl has been found to be the most abundant chlorine reservoir during PSC events, and its reaction with ClONO₂ on ice is thought to be the most important of the chlorine activation reactions:²



The reaction probability, γ , of reaction 1 on ice has been found in multiple laboratory studies to be high ($\gamma > 0.1$)^{2,4–10} and independent of HCl partial pressure (P_{HCl}), even when experiments cross the ice–liquid phase boundary into high HCl partial pressures which are known to induce melting of the ice sample.¹⁰

Clearly, characterization of the interaction of HCl with ice is one of the first steps toward understanding chlorine activation. Over the past 25 years, the HCl–ice system has been investigated using numerous experimental^{2,4,6,10–71} and theoretical^{71–104} approaches. While much uncertainty remains regarding the fate of HCl upon adsorption to ice, these studies have led to a consensus that HCl has a high affinity for ice surfaces, with near monolayer coverage at conditions relevant to PSC events (3×10^{-8} Torr $< P_{\text{HCl}} < 2 \times 10^{-7}$ Torr, 188 K $< T < 203$ K). Given the absence of direct experimental information about the state of the ice surface in the presence of HCl at these conditions, previous studies were conducted under the simplifying assumption that the ice surface is unchanging and refractory. With the assumption that HCl makes at most a very strong hydrogen bond with a refractory ice surface, calculations predict at least 2 orders of magnitude less HCl uptake than what has been observed.³

We showed in a recent study that trace amounts of HCl induce the formation of a disordered surface region on ice, or “quasiliquid layer” (QLL),^{105,106} at stratospheric temperatures.¹⁰⁷

[†] Department of Chemical Engineering.

[‡] Present affiliation: Department of Chemical Engineering, Columbia University, New York, NY 10027.

[§] Departments of Chemistry and Earth, Atmospheric, and Planetary Sciences.

^{||} Present affiliation: Department of Chemistry, Northwestern University, Evanston, IL 60208.

⁻ Present affiliation: Institute of Physical Chemistry, Institute of General, Inorganic, and Theoretical Chemistry, University of Innsbruck, A-6020 Innsbruck, Austria.

^{*} Present affiliation: Department of Chemistry and Biochemistry, University of California at San Diego, La Jolla, CA 92093-0356.

Further, we showed that the presence of this disordered surface enhances the chlorine activation reaction of HCl with chlorine nitrate (ClONO₂), and confirmed that the presence of surface disorder explains the catalytic role PSC particle surfaces play in chlorine activation. Interestingly, we only saw surface disorder induced at temperatures and HCl partial pressures in the vicinity of the solid–liquid equilibrium line on the HCl–ice phase diagram.

Here we present a detailed investigation of the interaction of HCl with a variety of ice surfaces using a flow tube with ice-coated walls coupled with chemical ionization mass spectrometry (CIMS) detection of the gas phase. Equipped with information from our recent study on the potential complexity of the HCl–ice surface system,¹⁰⁷ we have paid particular attention to the role of the QLL, as well as the degree of crystallinity and roughness of the ice samples used. The results of this study give new information about the fate of HCl upon adsorption to different types of ice under a wide range of conditions represented by the HCl–ice phase diagram, including conditions where HCl-induced disordering on ice was and was *not* observed using ellipsometry,¹⁰⁷ as well as HCl hexahydrate formation. These results provide new information on the complex dependence of the HCl–ice interaction on the surface roughness, polycrystallinity, and surface disordering of the substrate.

II. Experimental Section

A. Flow System and CIMS Detection. A schematic diagram of a typical experimental setup for the flow tube–CIMS experiments is available in the Supporting Information (SI). All flow tube–CIMS experiments employed a 2.5 cm i.d. flow tube (length 40 cm) operating in the laminar flow regime ($Re < 100$) that was interfaced with a CIMS system (Extrel C50). Detection occurred via chemical ionization using SF₆[−] as a reagent ion. SF₆[−] ions were generated in a sidearm attached at a right angle to the flow tube using a discharge needle operating at −4.8 kV. HCl was monitored as SF₅Cl[−] (162 amu).

All flows were monitored with calibrated flow meters (Tylan General). He (BOC gases) was used as a carrier gas. A 1600 L/min rotary pump (Edwards EM280) established flow velocities of 1000–2000 cm/s, with the corresponding Reynolds numbers well below the turbulence limit. The pressure inside the flow tube, measured with a 0–10 Torr MKS Baratron, was maintained constant during each experiment at approximately 1.5–2.0 Torr. A circulating cooler (Neslab ULT-95) was used to establish constant flow tube temperatures between 233 and 183 K. Cooling fluid flowed through the cooling jacket of the flow tube countercurrent to the gas flow. In all uptake experiments, a dilute mixture of each probe molecule of interest in He was introduced to the main He flow through a moveable injector positioned near the centerline of the flow tube.

The injectors were heated to prevent experimental artifacts due to adsorption of HCl to the injector walls. The temperature inside the flow tube was monitored using a copper/Constantan thermocouple (Omega). The thermocouple was housed in a 0.3 cm i.d. glass tube, which was inserted into the cooled region of the flow tube parallel to the injector. The axial location of the thermocouple was arbitrary since there were no temperature gradients greater than 1 K in the cooled region of the flow tube.

B. Water Vapor Pressure Measurements and Ice Film Preparation. In additional experiments, an electron impact residual gas analyzer (Ametek Dycor MA200 RGA) was used to measure the water vapor pressures of ice films between 188 and 195 K while they were being exposed to various HCl

pressures. The RGA was attached to a side port on the CIMS chamber. Water vapor was monitored via the oxygen ion signal at 16 amu. We calibrated the technique by monitoring the signal as a function of time while heating the ice film. The resulting water vapor pressure versus temperature curve agreed well with that reported by Marti and Mauersberger.¹⁰⁸ Three types of ice samples were used in this study: smooth ice films formed by quickly freezing from the melt,¹⁰⁹ vapor-deposited ice films,^{10,110} and zone-refined ice cylinders.¹⁰⁷ For ice preparation details, please refer to the SI.

C. General Procedure for HCl Uptake Experiments. Each uptake experiment began with the injector pushed to the front of the flow tube, past the ice sample, close to the CIMS region. A constant flow of HCl was established that corresponded to the desired HCl partial pressure, and the resulting baseline SF₅Cl[−] signal was recorded. The injector was then withdrawn, exposing the desired length of ice film to HCl. The resulting dip in the recorded signal reflects uptake of HCl to the ice sample. After the desired uptake time had passed, the injector was returned to the front of the flow tube, and the observed signal increase reflected the original baseline signal plus the signal from any desorbing HCl.

Surface coverage data was extracted from the uptake curves by numerically integrating to find the area between the curve and the baseline. To account for unknown irregularities at the front of the ice film, and any artifacts due to mixing at the tip of the injector, absolute surface coverages reported here are the coverage difference between two uptake curves for two different exposed areas. For example, the uptake measured with the injector positioned 4 cm from the front of the ice film would be subtracted from that measured with the injector at 10 cm, thus determining the coverage for the intermediate 6 cm. Reported uncertainties in surface coverage reflect the noise in the signal, which was carried through the arithmetic operations according to Jeffrey.¹¹¹

III. Results

A. HCl Adsorption on Smooth and Vapor-Deposited Ice. The uptake of HCl on smooth and vapor-deposited ice films was studied at 196, 203, and 213 K, and 5×10^{-8} Torr $< P_{\text{HCl}} < 3 \times 10^{-6}$ Torr. Figure 1 shows signal versus time traces for HCl uptake on smooth ice samples at 213 K and 7.4×10^{-7} Torr HCl (representative of non-disorder conditions, left) and 196 K and 10^{-6} Torr HCl (surface disorder conditions, right). Similar to what was observed previously for HCl adsorption on zone-refined ice,¹⁰⁷ we observed an initial fast mode of HCl adsorption, accounting for at least 75% of the total uptake within 180 s, followed by a slower uptake mode, with the signal returning to at least 95% of the baseline within 1000 s (see top panels in Figure 1). Our observations of an initial fast uptake mode followed by a diffusive-type loss for HCl adsorption on all ice films used in this study are consistent with the findings of other investigators.^{13,30}

Uptake experiments were performed at several HCl partial pressures and temperatures in order to gain insight into the adsorption mechanism. The measured adsorption isotherms for aged smooth ice surfaces are shown in Figure 2. Each point in Figure 2 corresponds to an average of at least 3 measured uptake values, often on multiple ice samples. Saturation surface coverage for the reversible adsorption mode (HCl exposure to aged ice surfaces) was measured to be $2\text{--}3 \times 10^{14}$ molecules cm^{−2} on smooth ice. The conditions at which we observed a transition to HCl-induced surface disordering in previous work are marked with dotted lines in Figure 2.¹⁰⁷ Our analysis of the

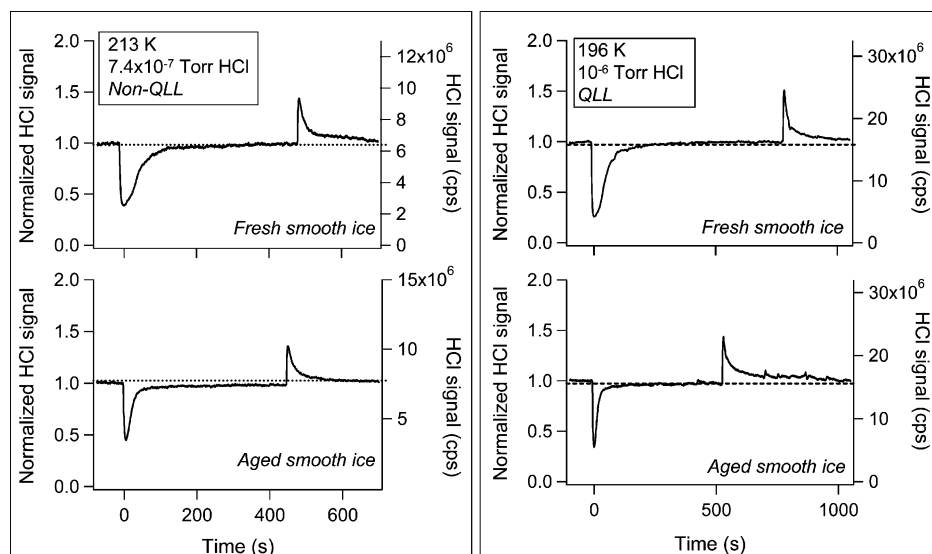


Figure 1. HCl uptake on smooth ice samples at 213 K and 7.4×10^{-7} Torr HCl (non-disorder conditions, left) and 196 K and 10^{-6} Torr HCl (surface disorder conditions, right). Each panel shows HCl mass spectrometer signal for an uptake experiment, with the normalized signal on the left axis and the raw signal on the right axis. The upper panels show adsorption onto “fresh” ice samples. The lower panels show adsorption for subsequent exposures (adsorption to “aged” ice samples).

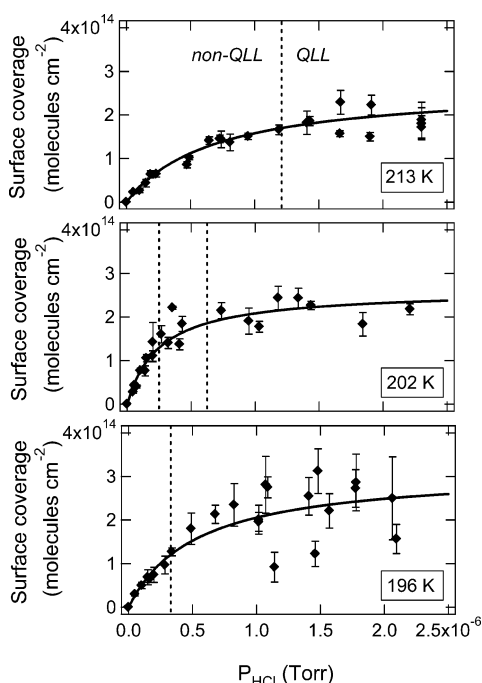


Figure 2. Adsorption isotherms for HCl on aged smooth ice at 213, 203, and 196 K. The dotted line demarcates the transition from non-disordered (non-QLL) to surface-disordering (QLL) levels of HCl at each temperature, based on the results of our previous work (note that data are unavailable for 202 K so an estimated range is provided).¹⁰⁷ Increased scatter was observed in the data under surface-disordering conditions. The Langmuir adsorption isotherm fits using “non-QLL” data only are indicated by the smooth lines. The error bars represent the standard deviation in the raw data used in the average.

adsorption isotherms and the role of surface disorder will be discussed in detail in the following sections.

We also carried out a detailed investigation of ice surface aging. For both smooth and vapor-deposited ice films, it was observed that, upon the first exposure of a fresh ice surface to HCl, only a fraction of the adsorbed HCl was recovered when the injector was returned to the front of the flow tube and

desorption was initiated. This suggests both reversible adsorption processes on the surface and processes that are irreversible on the time scale of the experiment. All subsequent exposures resulted in adsorption that was observed to be reversible on the time scale of the experiment (several minutes) (lower panels of Figure 1). In the experiments, the surface coverage was observed to be nearly constant and equal to the amount desorbed after the HCl source was removed for the second, third, and fourth exposures of an ice film to HCl. The aging effect was not observed to be reversible: after removing the HCl source for up to 1.5 h, additional HCl desorption was not detected, and in the next uptake experiment no additional irreversible uptake was observed. The uptake curve was typical of an ice surface that has been previously exposed to HCl rather than a refreshed ice surface. The aging effect was independent of P_{HCl} or type of ice sample. We define the aging ratio, χ , as the ratio of the measured surface coverage on an aged ice sample to the measured surface coverage for the first uptake experiment on that sample. For smooth ice at 213 K and 7.4×10^{-7} Torr HCl (non-disorder conditions), $\chi = 0.57 (\pm 0.03)$, and at 196 K and 1×10^{-6} Torr HCl (surface disorder conditions), $\chi = 0.50 (\pm 0.02)$. Each of these ratios is an average calculated from five aging experiments, with each experiment consisting of a sequence of four exposures (HCl adsorption and desorption). These observations are consistent with the results of others.^{6,13,29,30,112} Hanson and Ravishankara’s observation that HCl uptake decreased by approximately 50% after the first exposure of each ice sample to HCl is in good agreement with our findings.⁶ Our results are also in reasonable agreement with Hynes et al., who reported that up to 70% of incident HCl molecules were irreversibly adsorbed in their experiments on smooth ice at 205 K.²⁹

The only difference in uptake on smooth and vapor-deposited ice films was in the magnitude of observed uptake, which can be attributed to the higher surface area of the vapor-deposited ice.¹¹⁰ The HCl surface coverage for a $\sim 200 \mu\text{m}$ thick ice film deposited from the vapor phase at a rate of 4 mg min^{-1} was approximately 7 times greater than coverage on smooth ice at

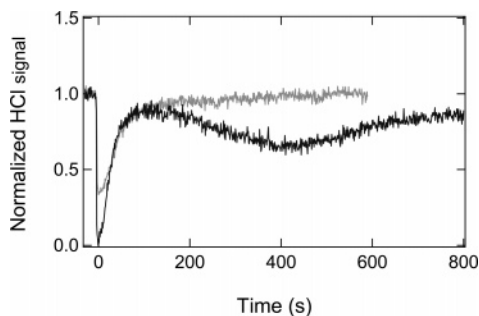


Figure 3. Normalized HCl mass spectrometer time traces for adsorption on smooth ice at 186 K. The gray trace was obtained for an HCl partial pressure of 3.9×10^{-7} Torr. The black trace, showing HCl uptake beyond surface saturation corresponding to HCl hexahydrate formation, was obtained for an HCl partial pressure of 5.8×10^{-7} Torr.

the same conditions. The surface area of the smooth ice films was assumed to be equal to the geometric area throughout the analysis.

B. HCl Hexahydrate Formation. On smooth ice films, at 186 K and HCl partial pressures above 4.5×10^{-7} Torr, we observed HCl losses beyond the expected profile for an adsorption/saturation process consistent with the formation of the HCl hexahydrate. Figure 3 shows uptake curves for HCl adsorption on smooth ice at 186 K for HCl partial pressures of 3.9×10^{-7} and 5.8×10^{-7} Torr. At 3.9×10^{-7} Torr, the uptake curve exhibits an initial fast adsorption mode followed by slower adsorption leading to saturation. At 5.8×10^{-7} Torr, which at 186 K lies in the region of the HCl–ice phase diagram where HCl hexahydrate is a metastable phase,²⁰ the same fast adsorption mode is observed initially. However, approximately 150 s after exposure a pronounced dip appears in the signal which is indicative of a secondary adsorption process. Uptake curves of this form were only found within the HCl hexahydrate stability region of the HCl–ice phase diagram.

We tested this secondary adsorption process to confirm that it was hexahydrate formation by measuring the water vapor pressure of several smooth ice films held between 188 and 195 K as a function of HCl partial pressure in the flow tube. At each ice film temperature, the water vapor pressure remained at the equilibrium ice vapor pressure for low P_{HCl} , and decreased for HCl partial pressures above the HCl hexahydrate stability line on the phase diagram, with slopes corresponding to the molar ratio of water to HCl (6:1) of the HCl hexahydrate (data not shown).

HCl uptake beyond saturation corresponding to HCl hexahydrate formation was also observed on zone-refined ice and on single-crystalline ice samples. HCl hexahydrate formation was not observed on vapor-deposited ice samples under any conditions. Figure 4 shows a summary of the results of several HCl uptake experiments on smooth, vapor-deposited, zone-refined, and single-crystal ice samples under the range of conditions known to produce HCl hexahydrate, superimposed on a detail of the HCl–ice phase diagram.³ The parallel dotted lines outline the range of conditions where HCl hexahydrate is a metastable phase.²⁰ Experiments performed on single-crystal ice samples were part of an ellipsometer-CIMS study published recently.¹⁰⁷ No experiments were performed at conditions in the HCl trihydrate regime.

IV. Discussion

A. HCl Adsorption on Ice (Non-QLL). 1. *Smooth and Vapor-Deposited Ice Films.* We first analyzed the non-QLL portion of our measured adsorption isotherms on smooth ice

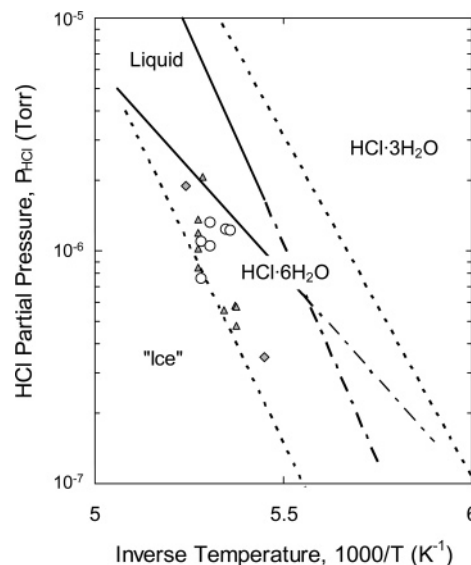


Figure 4. HCl hexahydrate formation for different types of ice surface. A summary of experimental results is superimposed on a detail of the HCl–ice phase diagram from Molina.³ Triangles represent experiments on smooth ice, circles represent experiments on vapor-deposited ice films, and diamonds represent experiments on zone-refined or single-crystalline ice samples. Filled symbols indicate observed HCl uptake beyond saturation corresponding to HCl hexahydrate formation, and open circles indicate no observed HCl hexahydrate formation. HCl hexahydrate formation was not observed on vapor-deposited ice films.

using the Langmuir model for surface adsorption (see, for example, Adamson).¹¹³ The parameters of the Langmuir model are the saturation surface coverage, S , and the surface adsorption equilibrium constant, b , defined as the ratio of the adsorption and desorption rate constants:

$$b = \frac{k_{\text{ads}}}{k_{\text{des}}} \quad (2)$$

To determine S and b at each temperature, the adsorption isotherm data obtained in the uptake experiments on smooth ice under non-QLL conditions were analyzed using a weighted linear least-squares fit according to

$$\frac{1}{c_s} = \frac{1}{S} + \frac{1}{S} \left(\frac{1}{bP_{\text{HCl}}} \right) \quad (3)$$

where c_s is the HCl surface coverage in molecules cm^{-2} . The uptake data for each temperature were tested to determine whether $1/c_s$ exhibited a linear dependence on $1/P_{\text{HCl}}$, or on $1/P_{\text{HCl}}^{1/2}$. Within the Langmuir framework, a $1/P_{\text{HCl}}^{1/2}$ dependence would imply that each adsorbed molecule would occupy two adjacent, identical adsorption sites (a simplified dissociative adsorption scenario). Such a dependence has been reported previously by other investigators.^{28–30} Chu et al. and Huthwelker et al. reported a $1/P_{\text{HCl}}^{1/2}$ dependence for uptake to vapor-deposited ice at HCl partial pressures that extended from the low P_{HCl} levels used in this study into the liquid regime.^{28,30} Hynes et al. used a $1/P_{\text{HCl}}^{1/2}$ model to describe data obtained on smooth ice in the saturation regime of the HCl uptake isotherm.²⁹ The results of this test for the 213 K adsorption isotherm are shown in Figure 5. Clearly, the linear $1/P_{\text{HCl}}^{1/2}$ model equation is a poor fit to the $1/c_s$ data, and results in nonphysical fit parameters: $S = -4 (\pm 2) \times 10^{14}$ molecules cm^{-2} , and $b = -8 (\pm 5) \times 10^4 \text{ Torr}^{-1}$. The linear $1/P_{\text{HCl}}$ model, eq 3, fits the $1/c_s$ data well, and the fit yields physically reasonable parameters: $S = 2.7 (\pm 0.2) \times 10^{14}$ molecules cm^{-2} ,

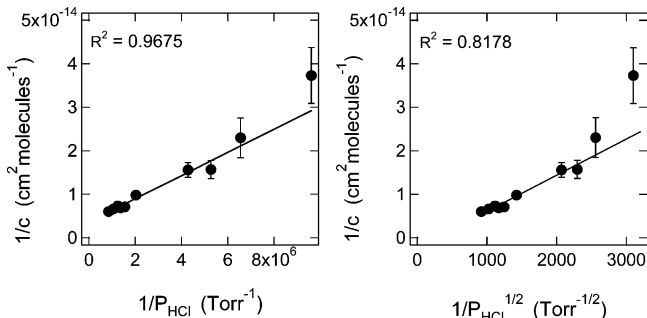


Figure 5. Langmuir fits of HCl adsorption data at 213 K. The inverse of the measured HCl surface coverage is plotted as a function of the inverse of the HCl partial pressure (left panel), and the same data is plotted as a function of the square root of the inverse of the HCl partial pressure (right panel). The lines indicate the results of weighted linear least-squares fits. The parameters for the $1/P_{\text{HCl}}^{1/2}$ fit are unphysical ($S = -4(2) \times 10^{14}$ molecules cm^{-2} , and $b = -8(\pm 5) \times 10^4$ Torr $^{-1}$), indicating that a $P_{\text{HCl}}^{1/2}$ Langmuir model is not appropriate for this system. The parameters for the $1/P_{\text{HCl}}$ fit are $S = 2.7(\pm 0.2) \times 10^{14}$ molecules cm^{-2} , and $b = 1.5(\pm 0.3) \times 10^6$ Torr $^{-1}$.

TABLE 1: Langmuir Parameters S (Saturation Surface Coverage) and b (Adsorption Equilibrium Constant) Calculated via Isotherm Analysis for HCl Adsorption on Smooth Ice Films for the Range of Conditions Where Surface Disorder Was Not Observed Using Ellipsometry^a

T (K)	S (molecules cm^{-2})	b (Torr $^{-1}$)
213	$2.7(\pm 0.2) \times 10^{14}$	$1.4(\pm 0.3) \times 10^6$
203	$2.6(\pm 0.4) \times 10^{14}$	$4(\pm 1) \times 10^6$
196	$3.1(\pm 0.9) \times 10^{14}$	$1.9(\pm 0.8) \times 10^6$

^a Errors are calculated according to Jeffrey.¹¹¹

and $b = 1.5(\pm 0.3) \times 10^6$ Torr $^{-1}$. Therefore, we conclude that the dissociative Langmuir model is not suitable under our experimental conditions, and that the data are better described at each temperature by the classical single-site Langmuir model. However, it is important to note that, in the absence of additional data, we cannot rule out dissociative adsorption. This is consistent with the findings of Ullerstam et al. for HNO₃ adsorption at submonolayer levels.¹¹² We performed a Langmuir analysis of the HCl adsorption isotherms we obtained on previously exposed smooth ice films (see Figure 2) for the range of conditions where surface disorder was not observed using ellipsometry. The saturation surface coverage, S , and the equilibrium adsorption constant, b , obtained are listed in Table 1.

Using the Van't Hoff relationship, the plot of $\ln(b)$ versus T^{-1} will be linear, and the slope of the line should yield energetic information according to

$$\ln b = -\frac{1}{T} \left(\frac{\Delta H_{\text{ads}}}{R} \right) + \frac{\Delta S_{\text{ads}}}{R} \quad (4)$$

where ΔH_{ads} and ΔS_{ads} are the enthalpy and entropy of adsorption, respectively, and R is the gas constant.¹¹⁴ Figure 6 shows $\ln(b)$ versus T^{-1} resulting from Langmuir fits to our HCl uptake data (see Table 1). We find that the dependence of our experimentally determined $\ln(b)$ values on inverse temperature is nonlinear, exhibiting somewhat poor agreement with eq 4. The overall slope corresponds to $\Delta H_{\text{ads}} = -15 \pm 2$ kJ mol $^{-1}$, consistent with nondissociative adsorption. For reference, the enthalpy of solution of HCl in liquid water, which includes ionization, is 75 kJ/mol.¹¹⁵ An isosteric heat of adsorption analysis of the data results in a

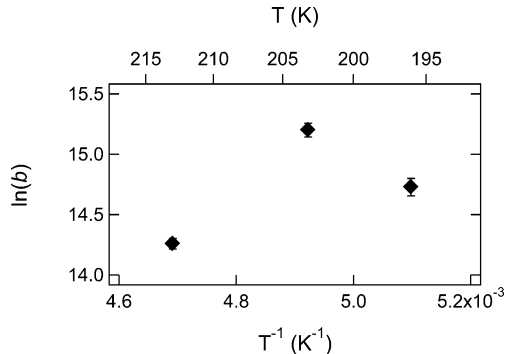


Figure 6. Temperature dependence of the Langmuir adsorption parameter for HCl adsorption on smooth ice films for the range of conditions where surface disorder was not observed using ellipsometry. The nonlinear dependence of $\ln(b)$ on T^{-1} indicates that ice is not a true Langmuir surface.

similar nonlinear dependence of $\ln(P_{\text{HCl}})$ on T^{-1} at constant surface coverage.¹¹³

The accuracy of this analysis is limited by the fact that we were only able to obtain three temperature points given our experimental constraints. However, due to the large number of experiments represented by the isotherms in Figure 2 (each point corresponds to an average of at least 3 measured uptake values), we believe that the observed disagreement with the Langmuir model is not solely attributable to reproducibility issues. One possible additional contribution to the apparent disagreement is that HCl-induced disordering may exist below the non-QLL/QLL boundary P_{HCl} values we have set based on our ellipsometer data, introducing error into Langmuir fits including data at those borderline values. One potential reason for this discrepancy is the difference in the ice sample preparation methods used in this study (zone-refined ice cylinders) and in the ellipsometer study (single-crystal ice samples). The conditions that lead to surface disordering may vary with crystal size or the density of grain boundaries in the ice sample. The limited ability of a model as simple as the Langmuir model to describe adsorption on the ice surface at all possible conditions, given what we know about its changeable nature, is not surprising. However, recognizing its limitations, the Langmuir model can be a useful tool in our analysis.

2. Numerical Modeling. To further investigate our experimental observations, a framework for numerical modeling of the flow tube experiments was developed. The model is similar in approach to that of Behr et al.¹¹⁶ and Cox et al.¹⁰⁴ The coated-wall flow tube was conceptually divided into a series of thin, radially well-mixed “slices”. This is a valid approximation because, in this system, radial diffusion is fast compared to axial convection. Gas-phase diffusion and convection in the axial direction were simulated, and a variety of models of solute interaction with the ice film were tested. More details regarding the model can be found in the SI. All simulations described were programmed and executed using MATLAB 6.0 (The MathWorks, Inc.). Simulation results are shown along with experimental data for comparison in Figures 7 and 9.

Using our flow tube modeling framework with a Langmuir model to describe the HCl–ice interaction, we can simulate both the shape of the uptake curves and the measured surface coverage for HCl uptake on smooth ice samples which had been previously exposed to HCl (“aged” samples). The results of the simulation are shown plotted along with the experimental data for comparison in the lower left panel of Figure 7. The total number of sites, S , was assumed to be the measured saturation

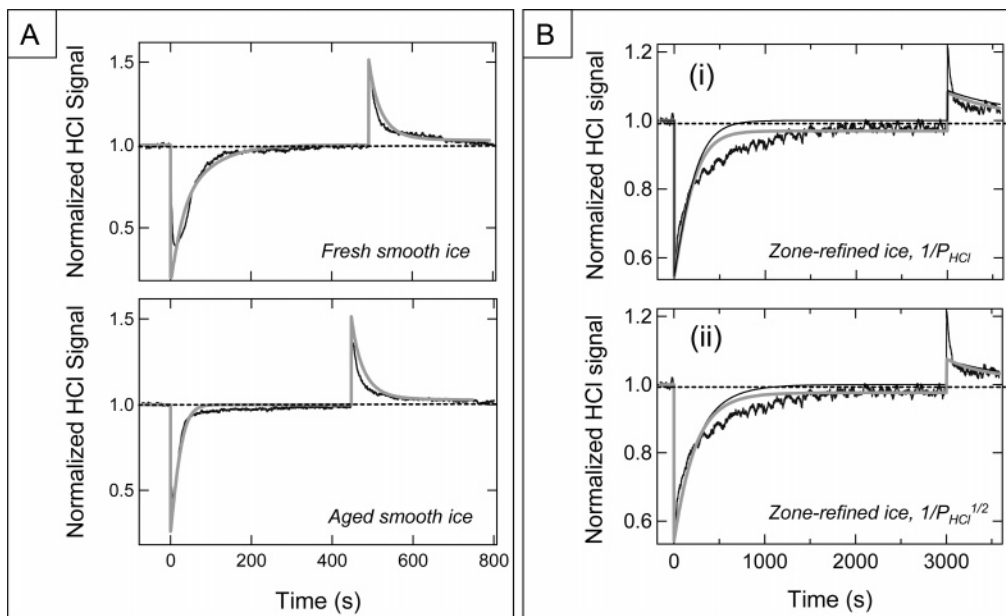


Figure 7. Flow tube model simulation results for adsorption of HCl onto smooth and zone-refined ice samples under non-QLL conditions (213 K, 7×10^{-7} Torr HCl). (A) Adsorption onto smooth ice. The upper panel shows adsorption onto a “fresh” ice sample, modeled using a two-site Langmuir model. The lower panel shows adsorption for subsequent exposures. (B) Adsorption onto zone-refined ice, modeled with (thick gray lines) and without (thin black lines) HCl diffusion into the bulk. The results of (i) a classical Langmuir model and (ii) a dissociative Langmuir model are shown. See text for details.

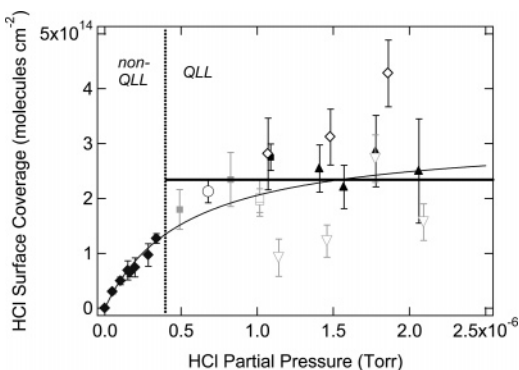


Figure 8. The effect of surface disorder on smooth ice samples. Shown is the measured adsorption isotherm for HCl on smooth ice at 196 K (from Figure 2). For surface disordering conditions, uptake data from the same ice sample have been represented using like symbols. The dotted line demarcates the transition to surface-disordering conditions ($P_{\text{HCl}} \sim 3 \times 10^{-7}$ Torr at 196 K). The Langmuir adsorption isotherm fit using “non-QLL” data only is indicated. The parameters for the fit are listed in Table 1. The horizontal line indicates the average surface coverage for surface disordering conditions, $2.11 (\pm 0.08) \times 10^{14}$ molecules cm^{-2} .

surface coverage (see Table 1). If adsorption is assumed to be barrierless, the adsorption rate constant, k_{ads} , is defined as

$$k_{\text{ads}} = \frac{\alpha}{S(2\pi mk_{\text{B}}T)^{1/2}} \quad (5)$$

where m is the molecular mass, k_{B} is the Boltzmann constant, and α is the mass accommodation coefficient.¹¹³ The desorption rate constant, k_{des} , was calculated from b and k_{ads} according to eq 2. In our models, α and b were adjustable parameters, but estimates of b are available from our isotherm analysis (see Table 1), and bounds can be placed on the value of α based on measurements available in the literature.^{14,29} Since radial diffusion is neglected in this model, the α values used in our simulation encompass both gas-phase diffusion and surface uptake.¹⁰⁴

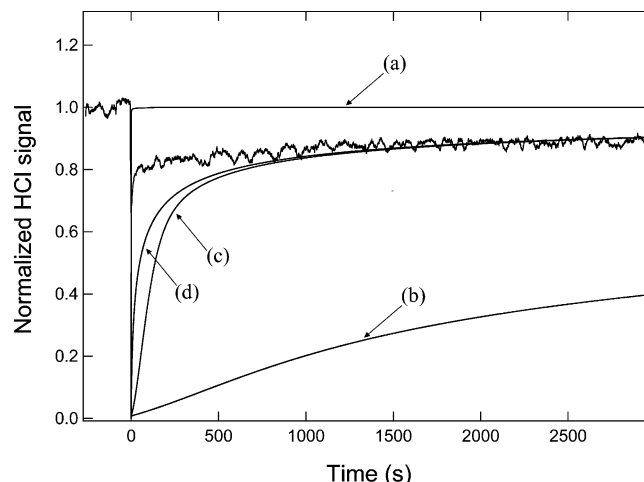


Figure 9. Simulations of the surface-to-bulk flux observed at long times upon HCl uptake to zone-refined ice under conditions where HCl-induced surface disorder was observed using ellipsometry in our previous work (196 K, 7×10^{-7} Torr).¹⁰⁷ Experimental data from our previous work are shown for comparison. Simulations were performed using the flow tube model framework and a model of absorption of HCl to (a) a bulk ice layer, (b) a true liquid layer, and a surface layer with $k_{\text{des}}(V_{\text{film}}/V_{\text{gas}}) = 1.5 \times 10^{-6} \text{ s}^{-1}$, which was (c) 100 nm thick and (d) 1 nm thick. All models account for diffusion from the surface layer to the bulk. The adsorption rate was calculated on the basis of gas kinetic theory, and the rates of desorption for ice and water were calculated using solubility data. Simulation results suggest that the surface-to-bulk flux observed at long times upon HCl uptake on zone-refined ice under QLL-forming conditions can best be described by absorption into a surface layer with an HCl solubility intermediate between that of a true liquid layer and bulk ice, regardless of layer thickness.

Hynes et al. measured an initial uptake coefficient, $\gamma \leq 0.05$, for HCl adsorption at $T > 205$ K and 1.1×10^{-6} Torr (conditions for which no surface change was observed in our ellipsometry experiments). The initial uptake coefficient can be taken as an approximation of α .¹¹⁷ For $T \leq 200$ K at similar HCl partial pressures (conditions where we observed surface

disordering in our ellipsometry experiments), Fluckiger et al. found that $\gamma \sim 0.1$.^{14,29,107} It should be noted that differences in ice sample preparation method could also contribute to the difference in observed uptake coefficients. On the basis of the best agreement with a sample of three measured uptake curves, we find that HCl adsorption on smooth ice at 213 K and non-QLL levels of HCl is described well by our model with $\alpha = 4.0 (\pm 0.1) \times 10^{-2}$ and $b = 1.0 (\pm 0.2) \times 10^6 \text{ Torr}^{-1}$. This value of b is consistent with the value obtained via isotherm analysis (see Table 1) and corresponds to a desorption rate constant, k_{des} , of $5 (\pm 1) \times 10^{-2} \text{ s}^{-1}$. This value of α is consistent with the findings of Hynes et al.²⁹ It was not necessary to include diffusion of HCl into the bulk in the model to reproduce the smooth ice adsorption curves with reasonable accuracy, although this does not rule out a small contribution of diffusive loss to the observed HCl uptake. The simulation predicts an equilibrium surface coverage of $1.2 \times 10^{14} \text{ molecules cm}^{-2}$, in close agreement with the measured surface coverage of $1.5 (\pm 0.2) \times 10^{14} \text{ molecules cm}^{-2}$.

The observed surface coverages and shapes of the adsorption and desorption curves for fresh ice not previously exposed to HCl, as shown in the top panels of Figure 1, can be reproduced to a reasonable approximation using a model that includes Langmuir adsorption of HCl to two types of adsorption sites: one set of sites identical to the model used to describe the adsorption curves on aged ice (lower left panel of Figure 7), and a second set of adsorption sites with stronger binding energy and a slightly lower sticking coefficient. A similar approach was used by Cox et al. to model HCl and HNO₃ adsorption on smooth ice films.¹⁰⁴ The simulation results for 213 K and $7.4 \times 10^{-7} \text{ Torr HCl}$ are shown in the top left panel of Figure 7 along with the experimental data for comparison. The best agreement with the observed amounts of adsorbed and desorbed HCl was obtained with $\alpha = 2.0 (\pm 0.1) \times 10^{-2}$ and $b = 2 (\pm 1) \times 10^7 \text{ Torr}^{-1}$ (corresponding to $k_{\text{des}} = 1.0 (\pm 0.5) \times 10^{-3} \text{ s}^{-1}$) for the second set of adsorption sites. The total number of weaker-binding sites was set equal to the measured saturation surface coverage for aged ice samples, S (see Table 1). The total number of stronger-binding sites, S_s , was calculated based on S and the experimentally determined aging ratio, χ , as follows:

$$S_s = S(1 - \chi^{-1}) \quad (6)$$

The simulation predicts a total HCl surface coverage (both site types) of $2.9 \times 10^{14} \text{ molecules cm}^{-2}$, in agreement with the measured first-exposure surface coverage of $3.1 (\pm 0.3) \times 10^{14} \text{ molecules cm}^{-2}$. The predicted ratio of desorbed HCl to adsorbed HCl was 0.6, which is close to the measured aging ratio, $\chi = 0.57 (\pm 0.03)$.

3. Zone-Refined Ice. In the range of conditions where surface disorder induction was not observed with ellipsometry, we observed largely irreversible HCl uptake on zone-refined ice. Furthermore, ClONO₂ + HCl reactive uptake experiments on zone-refined ice indicate that only a small fraction of the HCl adsorbed under these conditions is readily available on the surface for reaction with ClONO₂.¹⁰⁷ We used our modeling framework to gain further insight into the state of this apparently strongly adsorbed HCl. Within the numerical modeling framework, both (i) a model of Langmuir adsorption and (ii) a $P_{\text{HCl}}^{1/2}$ -dependence Langmuir model were tested against the experimental data. On the basis of our observations and work in the literature suggesting that diffusion from the surface to the bulk may be important,^{13–17,30,109} we tested these models with and without accounting for incorporation of HCl from the surface

into the bulk and diffusion to the interior of the film (see SI for details). We found that the best agreement between simulation and experiment for uptake curve shape and quantity of adsorbed molecules was achieved with the models that include incorporation and diffusion into the bulk.

The results of simulations i and ii are shown along with the experimental data in Figure 7b. On the basis of analysis of a sample of four measured uptake curves, we find that both models reproduce the uptake characteristics of HCl adsorption under non-QLL conditions on zone-refined ice reasonably well. This, along with the absence of adsorption isotherm data for this type of ice sample, means that neither model can be ruled out at this time. As noted above, a 1:1 relationship between adsorbed HCl molecules and surface sites does not rule out HCl dissociation.

The model parameters that resulted in the best agreement with the observed amounts of adsorbed and desorbed HCl were $\alpha = 1.2 (\pm 0.3) \times 10^{-2}$, $b = 8 (\pm 4) \times 10^6 \text{ Torr}^{-1}$, $S = 6 \times 10^{14} \text{ molecules cm}^{-2}$, and an incorporation rate constant (see SI), $k_{\text{inc}} = 4 (\pm 1) \times 10^{-4} \text{ s}^{-1}$ for simulation i. For simulation ii, $\alpha = 1.2 (\pm 0.3) \times 10^{-2}$, $b = 5 (\pm 3) \times 10^6 \text{ Torr}^{-1}$, and $k_{\text{inc}} = 4 (\pm 1) \times 10^{-4} \text{ s}^{-1}$. In simulation ii, each dissociated HCl molecule was assumed to occupy two identical surface sites, and the best agreement with experimental data was obtained with the total number of sites $S = 10^{15} \text{ molecules cm}^{-2}$. The calculated concentration of HCl in the near-surface region after 3000 s of adsorption was $6 \times 10^{-16} \text{ mol HCl cm}^{-3} \text{ ice}$ for simulation i and $4.5 \times 10^{-16} \text{ mol HCl cm}^{-3} \text{ ice}$ for simulation ii. Both of these values are many orders of magnitude less than the equilibrium solubility of HCl in bulk ice ($3.5 \times 10^{-7} \text{ mol HCl cm}^{-3}$).²⁶ Both simulations predict an uptake of $9.5 \times 10^{14} \text{ molecules cm}^{-2}$, compared with a measured value of $1.2 (\pm 0.1) \times 10^{15} \text{ molecules cm}^{-2}$, and both simulations reproduce the $1.7 (\pm 0.1) \times 10^{14} \text{ molecules cm}^{-2} \text{ HCl}$ that was recovered after 570 s of when the injector was returned to the front of the flow tube and desorption initiated. The HCl bulk incorporation rate constant of $4 (\pm 1) \times 10^{-4} \text{ s}^{-1}$, which provided the best agreement between simulation and experiment for both models, corresponds to a maximum surface-to-bulk loss rate of $2 \times 10^{11} \text{ molecules HCl cm}^{-2} \text{ s}^{-1}$, or 0.02% of the adsorbed HCl lost to the bulk per second.

B. Surface Disorder Conditions. *1. Smooth and Vapor-Deposited Ice Films.* Comparing the panels in Figure 1 demonstrates that, unlike what was observed on the zone-refined ice samples, there was no strong qualitative contrast found between the HCl uptake curves under QLL-forming versus non-QLL conditions for adsorption on smooth and vapor-deposited ices. However, for the range of HCl partial pressures where surface disorder was observed with ellipsometry, scatter in the uptake increased for each isotherm, and in the case of the 196 and 213 K isotherms, a unique dependence of uptake on HCl partial pressure for each ice sample became apparent. This is demonstrated in Figure 8, which shows the HCl adsorption isotherm for 196 K from Figure 2, but uptake data from the same ice sample have been represented using like symbols for surface disorder conditions.

2. Zone-Refined Ice. In our recent work on zone-refined ice in the “QLL” region of the HCl–ice phase diagram,¹⁰⁷ a nearly constant flux of $5 \times 10^{11} \text{ molecules HCl cm}^{-2} \text{ s}^{-1}$ from the surface to the interior of the ice sample was observed, which persisted throughout the time scale of the experiment (1 h). We used our flow tube model to further investigate this effect, comparing our experimental results to models of (a) absorption of HCl to a true liquid water layer, (b) adsorption to a bulk ice layer, and (c) adsorption to a surface layer with an HCl

solubility, and thus HCl desorption rate constant, intermediate between that of water and ice. In all cases the model accounted for diffusion from the surface layer into the bulk as described in the SI. The adsorption rate constant was calculated on the basis of gas kinetic theory assuming $\alpha = 0.1$, and the rate constants for desorption of HCl from ice and water were calculated on the basis of solubility data as follows: At equilibrium

$$k_{\text{ads}} \frac{P_{\text{HCl}}}{RT} = k_{\text{des}} [\text{HCl}]_{\text{sat}} \frac{V_{\text{film}}}{V_{\text{gas}}} \quad (7)$$

where V_{film} and V_{gas} are the film and gas volumes, respectively, and $[\text{HCl}]_{\text{sat}}$ is the equilibrium solubility. Note that, since when calculating k_{des} from equilibrium data for each ‘‘slice’’ along the axis of the flow tube, the rates are scaled with the ratio of the differential volume element of film to the differential volume element of gas, and are therefore dependent on the thickness of the surface layer. For bulk ice, $k_{\text{des}}(V_{\text{film}}/V_{\text{gas}}) = 5.2 \times 10^{-4} \text{ s}^{-1}$, based on a solubility of $3.5 \times 10^{-7} \text{ mol HCl cm}^{-3}$ ice at 200 K and 10^{-6} Torr HCl.²⁶ For liquid water, $k_{\text{des}}(V_{\text{film}}/V_{\text{gas}}) = 1.5 \times 10^{-7} \text{ s}^{-1}$, based on a solubility of 25% by weight at 196 K and 1.5×10^{-5} Torr HCl.³ In the simulations, the disordered surface layer was assumed to be ~ 100 nm thick.^{13,15,17,107}

The results of the simulations are shown in Figure 9 along with experimental data from our previous work for comparison.¹⁰⁷ HCl uptake on zone-refined ice under QLL-forming conditions can best be described at long times by HCl absorption into a surface layer with a desorption rate of $k_{\text{des}}(V_{\text{film}}/V_{\text{gas}}) = 1.5 \times 10^{-6} \text{ s}^{-1}$, intermediate between that of a true liquid layer and bulk ice. For $k_{\text{des}}(V_{\text{film}}/V_{\text{gas}}) = 1.5 \times 10^{-6} \text{ s}^{-1}$ and a surface layer 100 nm thick, assuming $\alpha = 0.1$, and $D_i = 10^{-12} \text{ cm}^2 \text{ s}^{-1}$, we find that, after 3000 s of exposure to gas-phase HCl, the near-surface concentration throughout the exposed area of the film reaches a value of approximately $9 \times 10^{-5} \text{ mol HCl cm}^{-3}$, and the diffusive flux from the near-surface region into the interior of the film is $5.3 \times 10^{11} \text{ molecules cm}^{-2} \text{ s}^{-1}$. The results of this analysis suggest that the surface-to-bulk loss we observe at long times can be explained in part by diffusion from a relatively concentrated surface layer into the bulk. This interpretation is consistent with those put forth by Huthwelker et al.³⁰ and Rossi and co-workers.^{13–17}

In our ellipsometry experiments,¹⁰⁷ surface disordering was observed to begin after a delay of 600 s. The model presented here only describes adsorption to and diffusion from a surface layer, and we have not made an attempt here to model QLL induction, or HCl adsorption to the surface prior to QLL formation. Therefore, comparison of model to experiment is only relevant after the 600 s induction period. Additionally, in our ellipsometry measurements,¹⁰⁷ the QLL thickness continued to increase for as long as the crystal was exposed to gas-phase HCl after QLL formation was initiated. It is important to note that, while each simulation assumes a surface layer of constant thickness, our model is insensitive to surface layer thickness at long times (see Figure 9c,d). This result is consistent with the notion that, regardless of the layer thickness, the same equilibrium near-surface concentration is achieved within a relatively short time. At long times, the surface-to-bulk diffusive flux, in eq S7 of the SI, is determined only by the near-surface concentration and the diffusivity. Therefore, we find that adsorption to a true liquid layer, even a very thin one, overestimates the observed surface-to-bulk flux of HCl at long times. Likewise, adsorption to a solid ice layer, even a very thick one, underestimates the observed surface-to-bulk flux of

HCl. A value of $k_{\text{des}}(V_{\text{film}}/V_{\text{gas}}) = 1.5 \times 10^{-6} \text{ s}^{-1}$, regardless of assumed value for α or layer thickness between 1 and 300 nm, corresponds to a solubility of $[\text{HCl}]_{\text{sat}} = 9.3 \times 10^{-5} \text{ mol HCl cm}^{-3}$ ice for the QLL at 196 K and 7×10^{-7} Torr HCl.

C. The Effect of Surface Roughness. Comparing our results for HCl adsorption on smooth versus vapor-deposited ice films allows us to observe the effects of varying surface roughness. In our measurements of HCl adsorption under non-surface-disorder conditions, the aging ratio, χ (vida supra), on fresh ice samples was not observed to be appreciably different for smooth ice films as compared with rough ice films formed by deposition from the vapor phase. The only observed difference in uptake on smooth and uptake on vapor-deposited ice films was in the magnitude of HCl uptake, which we have attributed to the higher surface area of the vapor-deposited ice.¹¹⁰

As shown in Figure 4, HCl hexahydrate formation was observed on smooth and zone-refined ice samples. However, HCl uptake beyond saturation corresponding to hexahydrate formation was not observed on vapor-deposited ice samples at the same conditions. Surface roughness is the characteristic that distinguishes vapor-deposited ice from the other two sample types.¹¹⁰ While the flow tube-CIMS technique offers only indirect information about the chemical state of HCl on the ice surface, this observation suggests that HCl hexahydrate formation at these conditions is a process involving hydrate nucleation and propagation on the crystal surface, rather than one originating in grain boundaries (abundant in polycrystalline ice), as has been suggested for ice formed at lower temperatures.³⁵ Our observations of an initial fast adsorption mode followed by a pronounced dip in the signal after approximately 150 s for HCl adsorption on smooth and zone-refined ice films in the region of the HCl-ice phase diagram where HCl hexahydrate is a metastable phase are consistent with the findings of other investigators that there is a nucleation barrier to HCl hexahydrate formation.^{10,20–23}

D. The Role of Domain Size. Qualitative and quantitative differences are observed when comparing HCl uptake on smooth and vapor-deposited ice films to uptake on the zone-refined ice samples. The key difference between the zone-refined ice cylinders and the other two film types is that the zone-refined ice cylinders have larger domain sizes, or fewer grain boundaries per unit surface area. The preparation method for the zone-refined ice cylinders involves very slow freezing, and results in crystal domains on the order of 1 cm. An additional distinguishing feature is that the zone-refined ice samples were thicker than the other two types of ice film. However, by analyzing diffusion through the bulk ice film it can be seen that only the topmost few microns of the ice film are penetrated within the time scale of the experiment, and so the three types of ice film effectively would have the same thickness (see the SI for details).

Table 2 lists the adsorption parameters obtained using our simulations for HCl adsorption under non-QLL conditions. Two of the three types of HCl adsorption that we have observed in our experiments under non-QLL conditions can be described as exhibiting strong binding: non-QLL adsorption to zone-refined ice cylinders, and the irreversible adsorption on fresh smooth ice cylinders. The weak binding mode was significant only for the more polycrystalline ice films studied. This suggests that the observed irreversible loss may be associated with adsorption onto the crystal face, and that reversible uptake can be attributed to adsorption into the grain boundaries. This is consistent with previous suggestions that HCl loading at the grain boundaries could lead to local disorder in the ice lattice.^{25,27}

TABLE 2: Adsorption Parameters Obtained via Simulations for HCl Adsorption to Smooth and Zone-Refined Ice Films at 213 K and Non-Surface-Disordering Levels of HCl^a

ice	model	α	k_{des} (s ⁻¹)	b (Torr ⁻¹)	k_{inc} (s ⁻¹)
aged smooth	Langmuir (weak binding)	$4.0 (\pm 0.1) \times 10^{-2}$	$5 (\pm 1) \times 10^{-2}$	$1.0 (\pm 0.2) \times 10^6$	N/A
fresh smooth	Langmuir (strong binding)	$2.0 (\pm 0.1) \times 10^{-2}$	$1.0 (\pm 0.5) \times 10^{-3}$	$2 (\pm 1) \times 10^7$	N/A
zone-refined	Langmuir	$1.2 (\pm 0.3) \times 10^{-2}$	$1.0 (\pm 0.5) \times 10^{-3}$	$8 (\pm 4) \times 10^6$	$4 (\pm 1) \times 10^{-4}$
zone-refined	dissociative Langmuir	$1.2 (\pm 0.3) \times 10^{-2}$	$1.0 (\pm 0.5) \times 10^{-3}$	$5 (\pm 3) \times 10^6$	$4 (\pm 1) \times 10^{-4}$

^a Relatively strong binding of HCl to the ice surface is associated with zone-refined ice cylinders and fresh smooth ice cylinders. Weaker binding is associated with aged ice cylinders.

In this scenario, the HCl-loaded, disordered grain boundaries could have properties similar to those of zone-refined ice samples which have been exposed to HCl under QLL-forming conditions;¹⁰⁷ they would exhibit largely reversible adsorption and act as a source of HCl that is readily available for reaction. However, to our knowledge no direct evidence exists, either in our work or in the literature, to support the picture of preferential adsorption leading to disordering at grain boundaries. In the absence of disordering at the grain boundaries, HCl molecules adsorbed there would be presumably less available for reaction than molecules adsorbed to the surface.

Short-lived cubic ice defects have been postulated to play a role in the uptake of acetone to primarily hexagonal ice samples.¹¹⁸ We observed significant irreversible HCl uptake and aging effects at all temperatures studied (196, 203, and 213 K), and for all ice sample types, from ice deposited from the vapor phase at 233 K to very slowly zone-refined ice cylinders. Therefore, we feel that it is not likely that short-lived cubic ice defects played a role in our observations.

V. Atmospheric Implications and Conclusions

It is expected that type II PSC particles consist of single ice crystals, because they grow slowly and at low temperatures.^{119,120} Therefore, we would expect the interaction of HCl with stratospheric ice particles to more closely resemble our observations on the single crystalline ice samples used in our CIMS-ellipsometry study¹⁰⁷ or the zone-refined ice cylinders than the two polycrystalline sample types studied here. However, the polycrystalline ice samples used here are typical of coated-wall flow tube studies.^{6,7,29,109,112} Clearly, the results of this study underscore the fact that investigators should exercise caution when extending observations made on laboratory ice surfaces to atmospheric ice systems.

In this work, we have quantitatively shown that the nature of the HCl–ice interaction is critically dependent on the characteristics of the ice substrate. Such a dependence has been noted previously,^{35,112,121,122} but our results reveal additional complexity in the relationship between observed HCl uptake and the ice surface roughness, history, polycrystallinity, and surface disordering. Characterization of the ice samples used in laboratory studies is essential for the interpretation of results, and understanding the physical state of ice in the environment is key to understanding its interactions with gas-phase species.

We have presented a detailed investigation of the interaction of HCl with three different ice substrates which allow us to observe the effects of surface roughness and the degree of crystallinity at a range of conditions including those found in the stratosphere. Numerical simulations applied to our experimental CIMS data indicate that HCl adsorption on polycrystalline ice films commonly used in laboratory studies consists of two modes: one relatively strong mode leading to adsorption that appears to be irreversible on a time scale of 30 min, and one relatively weak binding mode leading to reversible adsorption. We have indirect experimental evidence that these two

modes of adsorption correspond to adsorption to sites at crystal faces and those at grain boundaries, but there is not enough information to enable us to conclusively assign each adsorption mode to a type of site. At conditions where HCl-induced surface disorder is not anticipated, we have observed Langmuir-like submonolayer HCl adsorption on polycrystalline laboratory ice surfaces which have previously been exposed to HCl. However, the HCl–ice interaction is not well-described by a classical Langmuir model when comparing between temperatures. The predicted presence of the QLL and the domain size (i.e., density of grain boundaries) in the ice sample both control HCl uptake. Finally, we found indirect evidence that HCl hexahydrate formation on ice between 3×10^{-7} and 2×10^{-6} Torr HCl and between 186 and 190 K is a process involving hydrate nucleation and propagation on the crystal surface.

Acknowledgment. This research was supported by grants from the National Aeronautics and Space Administration (NASA) and the National Science Foundation (NSF). We also wish to acknowledge a NASA Graduate Student Fellowship in Earth System Science (V.F.M.), the Austrian Science Fund Schrödinger Fellowship (T.L.), and the National Oceanographic and Atmospheric Administration Postdoctoral Program in Climate and Global Change (F.M.G.) for support.

Supporting Information Available: Figure S1 of the experimental setup, discussion of ice film preparation and the flow tube model, Figure S2 of the time evolution of the concentration depth profile, Figure S3 of J vs time, Figure S4 of the numerical modeling of the flow tube model. This material is available free of charge via the Internet at <http://pubs.acs.org>.

References and Notes

- (1) Solomon, S.; Garcia, R. R.; Rowland, F. S.; Wuebbles, D. J. *Nature* **1986**, *321*, 755–758.
- (2) Molina, M. J.; Tso, T. L.; Molina, L. T.; Wang, F. C. Y. *Science* **1987**, *238*, 1253–1257.
- (3) Molina, M. J. *The Chemistry of the Atmosphere: The Impact of Global Change*; Blackwell Scientific Publications: Boston, 1994; Chapter 3, pp 27–38.
- (4) Leu, M. T. *Geophys. Res. Lett.* **1988**, *15*, 17–20.
- (5) Abbatt, J. P. D.; Molina, M. J. *Geophys. Res. Lett.* **1992**, *19*, 461–464.
- (6) Hanson, D. R.; Ravishankara, A. R. *J. Phys. Chem.* **1992**, *96*, 2682–2691.
- (7) Chu, L. T.; Leu, M. T.; Keyser, L. F. *J. Phys. Chem.* **1993**, *97*, 12798–12804.
- (8) Oppliger, R.; Allanic, A.; Rossi, M. J. *J. Phys. Chem. A* **1997**, *101*, 1903–1911.
- (9) Lee, S. H.; Leard, D. C.; Zhang, R.; Molina, L. T.; Molina, M. J. *Chem. Phys. Lett.* **1999**, *315*, 7–11.
- (10) Abbatt, J. P. D.; Beyer, K. D.; Fucaloro, A. F.; McMahon, J. R.; Wooldridge, P. J.; Zhang, R.; Molina, M. J. *J. Geophys. Res.* **1992**, *97*, 15819–15826.
- (11) Abbatt, J. P. D. *Chem. Rev.* **2003**, *103*, 4783–4800.
- (12) Demirdjian, B.; Ferry, D.; Suzanne, J.; Toubin, C.; Picaud, S.; Hoang, P. N. M.; Girardet, C. *J. Chem. Phys.* **2002**, *116*, 5143–5149.
- (13) Fluckiger, B.; Chaix, L.; Rossi, M. J. *J. Phys. Chem. A* **2000**, *104*, 11739–11750.

- (14) Fluckiger, B.; Thielmann, A.; Gutzwiller, L.; Rossi, M. *J. Ber. Bunsen-Ges. Phys. Chem.* **1998**, *102*, 915–928.
- (15) Aguzzi, A.; Fluckiger, B.; Rossi, M. *J. Phys. Chem. Chem. Phys.* **2003**, *5*, 4157–4169.
- (16) Fluckiger, B.; Rossi, M. *J. Phys. Chem. A* **2003**, *107*, 4103–4115.
- (17) Fluckiger, B.; Chaix, L.; Rossi, M. *J. Phys. Chem. A* **2003**, *107*, 2768.
- (18) Diehl, K.; Mitra, S. K.; Pruppacher, H. R. *Atmos. Res.* **1998**, *47–48*, 235–244.
- (19) Wofsy, S. C.; Molina, M. J.; Salawitch, R. J.; Fox, L. E.; McElroy, M. B. *J. Geophys. Res.—Atmos.* **1988**, *93*, 2442–2450.
- (20) Hanson, D. R.; Mauersberger, K. *J. Phys. Chem.* **1990**, *94*, 4700–4705.
- (21) Henson, B. F.; Wilson, K. R.; Robinson, J. M.; Noble, C. A.; Casson, J. L.; Worsnop, D. R. *J. Chem. Phys.* **2004**, *121*, 8486–8499.
- (22) Wooldridge, P. J.; Zhang, R.; Molina, M. J. *J. Geophys. Res.* **1995**, *100*, 1389–96.
- (23) Foster, K. L.; Tolbert, M. A.; George, S. M. *J. Phys. Chem. A* **1997**, *101*, 4979–4986.
- (24) Xueref, I.; Domine, F. *Atmos. Chem. Phys.* **2003**, *3*, 1779–1789.
- (25) Wolff, E. W.; Mulvaney, R.; Oates, K. *Geophys. Res. Lett.* **1989**, *16*, 487–490.
- (26) Thibert, E.; Domine, F. *J. Phys. Chem. B* **1997**, *101*, 3554–3565.
- (27) Krieger, U. K.; Huthwelker, T.; Daniel, C.; Weers, U.; Peter, T.; Lanford, W. A. *Science* **2002**, *295*, 1048–1050.
- (28) Chu, L. T.; Leu, M. T.; Keyser, L. F. *J. Phys. Chem.* **1993**, *97*, 7779–7785.
- (29) Hynes, R. G.; Mossinger, J. C.; Cox, R. A. *Geophys. Res. Lett.* **2001**, *28*, 2827–2830.
- (30) Huthwelker, T.; Malmstrom, M. E.; Helleis, F.; Moortgat, G. K.; Peter, T. *J. Phys. Chem. A* **2004**, *108*, 6302–6318.
- (31) Graham, J. D.; Roberts, J. T. *Geophys. Res. Lett.* **1995**, *22*, 251–254.
- (32) Graham, J. D.; Roberts, J. T. *Chemom. Intell. Lab. Syst.* **1997**, *37*, 139–148.
- (33) Graham, J. D.; Roberts, J. T. *J. Phys. Chem.* **1994**, *98*, 5974–83.
- (34) Roberts, J. T. *Acc. Chem. Res.* **1998**, *31*, 415–421.
- (35) Sadtchenko, V.; Giese, C. F.; Gentry, W. R. *J. Phys. Chem. B* **2000**, *104*, 9421–9429.
- (36) Isakson, M. J.; Sitz, G. O. *J. Phys. Chem. A* **1999**, *103*, 2044–2049.
- (37) Andersson, P. U.; Nagard, M. B.; Pettersson, J. B. C. *J. Phys. Chem. B* **2000**, *104*, 1596–1601.
- (38) Rieley, H.; Aslin, H. D. *J. Chem. Soc., Faraday Trans.* **1995**, *91*, 2349–51.
- (39) Koehler, B. G.; McNeill, L. S.; Middlebrook, A. M.; Tolbert, M. A. *J. Geophys. Res.—Atmos.* **1993**, *98*, 10563–10571.
- (40) Kang, H.; Shin, T. H.; Park, S. C.; Kim, I. K.; Han, S. J. *J. Am. Chem. Soc.* **2000**, *122*, 9842–9843.
- (41) Kondo, M.; Kawanowa, H.; Gotoh, Y.; Souda, R. *J. Chem. Phys.* **2004**, *121*, 8589–8593.
- (42) Horn, A. B.; Sodeau, J. R.; Roddis, T. B.; Williams, N. A. *J. Phys. Chem. A* **1998**, *102*, 6107–6120.
- (43) Koch, T. G.; Banham, S. F.; Sodeau, J. R.; Horn, A. B.; McCoustra, M. R. S.; Chesters, M. A. *J. Geophys. Res.—Atmos.* **1997**, *102*, 1513–1522.
- (44) Delzeit, L.; Devlin, M. S.; Rowland, B.; Devlin, J. P.; Buch, V. *J. Phys. Chem.* **1996**, *100*, 10076–10082.
- (45) Devlin, J. P.; Uras, N.; Sadlej, J.; Buch, V. *Nature* **2002**, *417*, 269–271.
- (46) Gilbert, A. S.; Sheppard, N. *J. Chem. Soc., Faraday Trans. 2* **1973**, *69*, 1628–1642.
- (47) Bournel, F.; Mangeney, C.; Tronc, M.; Laffon, C.; Parent, P. *Surf. Sci.* **2003**, *528*, 224–229.
- (48) Bournel, F.; Mangeney, C.; Tronc, M.; Laffon, C.; Parent, P. *Phys. Rev. B* **2002**, *65*, 201404–1.
- (49) Banham, S. F.; Sodeau, J. R.; Horn, A. B.; McCoustra, M. R. S.; Chesters, M. A. *J. Vac. Sci. Technol., A* **1996**, *14*, 1620–1626.
- (50) Barone, S. B.; Zondlo, M. A.; Tolbert, M. A. *J. Phys. Chem. A* **1999**, *103*, 9717–9730.
- (51) Buch, V.; Sadlej, J.; Aytemiz-Uras, N.; Devlin, J. P. *J. Phys. Chem. A* **2002**, *106*, 9374–9389.
- (52) Uras-Aytemiz, N.; Joyce, C.; Devlin, J. P. *J. Phys. Chem. A* **2001**, *105*, 10497–10500.
- (53) Donsig, H. A.; Vickerman, J. C. *J. Chem. Soc., Faraday Trans.* **1997**, *93*, 2755–2761.
- (54) Haq, S.; Harnett, J.; Hodgson, A. *J. Phys. Chem. B* **2002**, *106*, 3950–3959.
- (55) Banham, S. F.; Horn, A. B.; Koch, T. G.; Sodeau, J. R. *Faraday Discuss.* **1995**, 321–332.
- (56) Horn, A. B.; Chesters, M. A.; McCoustra, M. R. S.; Sodeau, J. R. *J. Chem. Soc., Faraday Trans.* **1992**, *88*, 1077–1078.
- (57) Horn, A. B.; Sully, J. *J. Chem. Soc., Faraday Trans.* **1997**, *93*, 2741–2746.
- (58) Leutwyler, S. *Nature* **2002**, *417*, 230–231.
- (59) Livingston, F. E.; George, S. M. *J. Phys. Chem. A* **1998**, *102*, 10280–10288.
- (60) Livingston, F. E.; George, S. M. *J. Phys. Chem. A* **2001**, *105*, 5155–5164.
- (61) Livingston, F. E.; George, S. M. *J. Phys. Chem. A* **2002**, *106*, 5114–5119.
- (62) MacTaylor, R. S.; Gilligan, J. J.; Moody, D. J.; Castleman, A. W. *J. Phys. Chem. A* **1999**, *103*, 4196–4201.
- (63) Persiantseva, N. M.; Popovicheva, O. B.; Rakhimova, T. V. *Chem. Phys. Rep.* **1998**, *17*, 543–559.
- (64) Persiantseva, N. M.; Popovicheva, O. B.; Rakhimova, T. V. *Surf. Rev. Lett.* **1998**, *5*, 437–441.
- (65) Peter, T. *Annu. Rev. Phys. Chem.* **1997**, *48*, 785–822.
- (66) Domine, F.; Rauzy, C. *Atmos. Chem. Phys.* **2004**, *4*, 2513–2519.
- (67) Parent, P.; Laffon, C. *J. Phys. Chem. B* **2005**, *109*, 1547–1553.
- (68) Devlin, J. P.; Gulluru, D. B.; Buch, V. *J. Phys. Chem. B* **2005**, *109*, 3392–3401.
- (69) Park, S. C.; Kang, H. *J. Phys. Chem. B* **2005**, *109*, 5124–5132.
- (70) Fernandez, M. A.; Hynes, R. G.; Cox, R. A. *J. Phys. Chem. A* **2005**, *109*, 9986–9996.
- (71) Ortega, I. K.; Escribano, R.; Herrero, V. J.; Mate, B.; Moreno, M. A. *J. Mol. Struct.* **2005**, *742*, 147–152.
- (72) Girardet, C.; Toubin, C. *Surf. Sci. Rep.* **2001**, *44*, 159–238.
- (73) Mantz, Y. A.; Geiger, F. M.; Molina, L. T.; Molina, M. J.; Trout, B. L. *Chem. Phys. Lett.* **2001**, *348*, 285–292.
- (74) Mantz, Y. A.; Geiger, F. M.; Molina, L. T.; Molina, M. J.; Trout, B. L. *J. Phys. Chem. A* **2001**, *105*, 7037–7046.
- (75) Bussolin, G.; Casassa, S.; Pisani, C.; Ugliengo, P. *J. Chem. Phys.* **1998**, *108*, 9516–9528.
- (76) Bacelo, D. E.; Binning, R. C.; Ishikawa, Y. *J. Phys. Chem. A* **1999**, *103*, 4631–4640.
- (77) Geiger, F. M.; Hicks, J. M.; de Dios, A. C. *J. Phys. Chem. A* **1998**, *102*, 1514–1522.
- (78) Hannachi, Y.; Silvi, B.; Bouteiller, Y. *J. Chem. Phys.* **1991**, *94*, 2915–2922.
- (79) Gertner, B. J.; Hynes, J. T. *Faraday Discuss.* **1998**, 301–322.
- (80) Packer, M. J.; Clary, D. C. *J. Phys. Chem.* **1995**, *99*, 14323–14333.
- (81) Re, S.; Osamura, Y.; Suzuki, Y.; Schaefer, H. F. *J. Chem. Phys.* **1998**, *109*, 973–977.
- (82) Svanberg, M.; Pettersson, J. B. C.; Bolton, K. *J. Phys. Chem. A* **2000**, *104*, 5787–5798.
- (83) Robertson, S. H.; Clary, D. C. *Faraday Discuss.* **1996**, *100*, 309–320.
- (84) Toubin, C.; Hoang, P. N. M.; Picaud, S.; Girardet, C. *Chem. Phys. Lett.* **2000**, *329*, 331–335.
- (85) Wang, T. X.; Margerum, D. W. *Inorg. Chem.* **1994**, *33*, 1050–1055.
- (86) Gertner, B. J.; Peshlherbe, G. H.; Hynes, J. T. *Isr. J. Chem.* **1999**, *39*, 273–281.
- (87) Calatayud, M.; Courmier, D.; Minot, C. *Chem. Phys. Lett.* **2003**, *369*, 287–292.
- (88) Casassa, S. *Chem. Phys. Lett.* **2000**, *321*, 1–7.
- (89) Bolton, K.; Pettersson, J. B. C. *J. Am. Chem. Soc.* **2001**, *123*, 7360–7363.
- (90) Clary, D. C.; Wang, L. C. *J. Chem. Soc., Faraday Trans.* **1997**, *93*, 2763–2767.
- (91) Al Halabi, A.; Kleyn, A. W.; Kroes, G. J. *J. Chem. Phys.* **2001**, *115*, 482–491.
- (92) Gardner, D. O. N.; Al Halabi, A.; Kroes, G. J. *Chem. Phys. Lett.* **2003**, *376*, 581–587.
- (93) Kroes, G. J.; Clary, D. C. *J. Phys. Chem.* **1992**, *96*, 7079–88.
- (94) Kroes, G. J.; Clary, D. C. *Geophys. Res. Lett.* **1992**, *19*, 1355–8.
- (95) Milet, A.; Struniewicz, C.; Moszynski, R.; Wormer, P. E. S. *J. Chem. Phys.* **2001**, *115*, 349–356.
- (96) Shevkunov, S. V. *JETP Lett.* **2003**, *76*, 700–703.
- (97) Toubin, C.; Picaud, S.; Hoang, P. N. M.; Girardet, C.; Demirdjian, B.; Ferry, D.; Suzanne, J. *J. Chem. Phys.* **2002**, *116*, 5150–5157.
- (98) Vakarin, E. V.; Holovko, M. F. *Chem. Phys. Lett.* **2001**, *349*, 13–18.
- (99) Vakarin, E. V.; Holovko, M. F.; Badiali, J. P. *Condens. Matter Phys.* **2001**, *26*, 251–260.
- (100) Vakarin, E. V.; Badiali, J. P.; Holovko, M. F. *Chem. Phys. Lett.* **2002**, *359*, 349–353.
- (101) Wang, L.; Clary, D. C. *J. Chem. Phys.* **1996**, *104*, 5663–73.
- (102) Woittequand, S.; Toubin, C.; Pouilly, B.; Monnerville, M.; Briquez, S.; Meyer, H. D. *Chem. Phys. Lett.* **2005**, *406*, 202–209.
- (103) Bianco, R.; Hynes, J. T. *Acc. Chem. Res.* **2006**, *39*, 159–165.
- (104) Cox, R. A.; Fernandez, M. A.; Symington, A.; Ullerstam, M.; Abbott, J. P. D. *J. Phys. Chem. Chem. Phys.* **2005**, *7*, 3434–3442.

- (105) Dash, J. G.; Fu, H.; Wettlaufer, J. S. *Rep. Prog. Phys.* **1995**, *58*, 115–67.
- (106) Petrenko, V. F.; Whitworth, R. W. *Physics of Ice*; Oxford University Press: New York, 1999.
- (107) McNeill, V. F.; Loerting, T.; Geiger, F. M.; Trout, B. L.; Molina, L. T.; Molina, M. J. *Proc. Natl. Acad. Sci. U.S.A.* **2006**, *103*, 9522–9427.
- (108) Marti, J.; Mauersberger, K. *Geophys. Res. Lett.* **1993**, *20*, 363–366.
- (109) Abbatt, J. P. D. *Geophys. Res. Lett.* **1997**, *24*, 1479–1482.
- (110) Leu, M. T.; Keyser, L. F.; Timonen, R. S. *J. Phys. Chem. B* **1997**, *101*, 6259–6262.
- (111) Jeffrey, A. *Mathematics for Engineers and Scientists*; Nelson: London, 1969.
- (112) Ullerstam, M.; Thornberry, T.; Abbatt, J. P. D. *Faraday Discuss.* **2005**, *130*, 211–226.
- (113) Adamson, A. W. *Physical Chemistry of Surfaces*, 5th ed.; Wiley: New York, 1990.
- (114) Steinfeld, J. I.; Francisco, J. S.; Hase, W. L. *Chemical Kinetics and Dynamics*, 2nd ed.; Prentice Hall: Upper Saddle River, NJ, 1999.
- (115) Atkins, P. W. *Physical Chemistry*, 5th ed.; W. H. Freeman & Co.: New York, 1994.
- (116) Behr, P.; Terziyski, A.; Zellner, R. *Z. Phys. Chem.* **2004**, *218*, 1307–1327.
- (117) Huthwelker, T.; Ammann, M.; Peter, T. *Chem. Rev.* **2006**, *106*, 1375–1444.
- (118) Behr, P.; Terziyski, A.; Zellner, R. *J. Phys. Chem. A* **2006**, *110*, 8098–8107.
- (119) Turco, R. P.; Toon, O. B.; Hamill, P. J. *Geophys. Res.—Atmos.* **1989**, *94*, 16493–16510.
- (120) Pueschel, R. F.; Snetsinger, K. G.; Goodman, J. K.; Toon, O. B.; Ferry, G. V.; Oberbeck, V. R.; Livingston, J. M.; Verma, S.; Fong, W.; Starr, W. L.; Chan, K. R. *J. Geophys. Res.—Atmos.* **1989**, *94*, 11271–11284.
- (121) Keyser, L. F.; Leu, M. T.; Moore, S. B. *J. Phys. Chem.* **1993**, *97*, 2800–2801.
- (122) Hanson, D. R.; Ravishankara, A. R. *J. Phys. Chem.* **1993**, *97*, 2802–2803.